Struct Multidisc Optim (2009) 38:331–346
DOI 10.1007/s00158-008-0299-3

RESEARCH PAPER

Application of maximum entropy principle for reliability-based design optimization

Hee Youb Kang · Byung Man Kwak

Received: 16 March 2008 / Revised: 3 June 2008 / Accepted: 5 July 2008 / Published online: 19 August 2008

Abstract The maximum entropy principle (MEP) is used to generate a natural probability distribution among the many possible that have the same moment conditions. The MEP can accommodate higher order moment information and therefore facilitate a higher quality PDF model. The performance of the MEP for PDF estimation is studied by using more than four moments. For the case with four moments, the results are compared with those by the Pearson system. It is observed that as accommodating higher order moment, the estimated PDF converges to the original one. A sensitivity analysis formulation of the failure probability based on the MEP is derived for reliability-based design optimization (RBDO) and the accuracy is compared with that by finite difference method (FDM). Two RBDO examples including a realistic three-dimensional wing design are solved by using the derived sensitivity formula and the MEP-based moment method. The results are compared with other methods such as TR-SQP, FAMM + Pearson system, FFMM + Pearson system in terms of accuracy and efficiency. It is also shown that an improvement in the accuracy by including more moment terms can increase numerical efficiency of optimization for the three-dimensional wing design. The moment method equipped with the MEP is found flexible and well adoptable for reliability analysis and design.

Keywords Maximum entropy principle · Moment method · Reliability-based design optimization

H. Y. Kang · B. M. Kwak (✉)
Korea Advanced Institute of Science and Technology, Daejeon, South Korea
e-mail: bmkwak@khp.kaist.ac.kr

Abbreviations

CDF	Cumulative Density Function
DoE	Design of Experiment
FAMM	Function Approximation Moment Method
FFMM	Full Factorial Moment Method
FORM	First Order Reliability Method
IMBQR	Improved Moment-Based Quadrature Rule
MBQR	Moment-Based Quadrature Rule
MCS	Monte Carlo Simulation
MEP	Maximum Entropy Principle
MPP	Most Probable failure Point
PDF	Probability Density Function
RBDO	Reliability-Based Design Optimization
SQP	Sequential Quadratic Programming
TR-SQP	Trust Region-Sequential Quadratic Programming

1 Introduction

Among the methods for quantitative assessment of reliability, the first order reliability methods (FORM; Hasofer and Lind 1974; Rackwitz and Fiessler 1978) and the moment methods (D'Errico and Zaino 1988; Zhao and Ono 2001; Seo and Kwak 2002; Lee and Kwak 2006; Huh and Kwak 2006; Huang and Du 2006; Ju and Lee 2007) are widely used. In FORM, a performance function is linearized at the most probable failure point (MPP), which is the closest point to the origin in the reduced variable space (Hasofer and Lind 1974). The probability can be obtained by using the relationship between the reliability index denoting the distance and the cumulative density function (CDF) of standard normal distribution. FORM is considered the

most efficient and the most easily implementable for practical problems. However, it has drawbacks such as the degradation of accuracy resulted from the multiple MPPs, the non-linearity of the performance function or the non-normality of random variables (Hasofer and Lind 1974; Rackwitz and Fiessler 1978). In the moment methods, the failure probability is calculated through a moment evaluation process and a PDF modeling process (Zhao and Ono 2001; Seo and Kwak 2002). Compared with FORM, moment methods have the advantages that they do not involve the difficulties of the MPP search and the information of CDF or PDF is readily available.

In the moment-based approaches, how to efficiently obtain the moments have been the main concern in previous studies but there has been relatively little concern about which modeling method gives the most appropriate PDF for reliability analysis. Until now the PDF is usually modeled by the polynomial normal transformation (Chen and Tung 2003), the saddle point approximation (Huang and Du 2006) and the Pearson system (Zhao and Ono 2001; Seo and Kwak 2002; Lee and Kwak 2006; Huh and Kwak 2006; Ju and Lee 2007), which is most frequently used and also known as the most accurate method among the empirical distribution systems such as the Johnson system, Gram–Charlier series, and so on (Johnson et al. 1994). The Pearson system uses only the first four moments of a performance function to determine its PDF. However, the PDF estimated by the Pearson system is not the only one that fits the given moment conditions and therefore the failure probability of the given performance function is also not unique. Also, how to generally estimate the PDF model for a given set of moments is an important issue in moment-based reliability analysis.

In the present paper, the maximum entropy principle (MEP; Shannon 1948; Jaynes 1957) is introduced for PDF modeling and RBDO application. The sensitivity analysis of the failure probability evaluated by MEP is then performed and compared with the sensitivity obtained by finite difference method (FDM). RBDO examples are also solved by the proposed method and other RBDO methods. The PDFs in the RBDO examples are obtained using the first four or five moments and the five integration points are used to calculate the moments of the performance function. The RBDO results by MEP using FFMM are compared with other reliability analysis methods such as FORM, FFMM + Pearson system and function approximation moment method (FAMM) + Pearson system (Huh and Kwak 2006). Pre-assumption in this study is that the given moments are accurately obtained by a general level Gauss quadrature method, which is known as moment-based quadrature rule (MBQR; Rahman and Xu 2004).

2 Reviews on moment calculation method

For a random variable x, the k-th order raw moment of a performance function, $g(x)$, can be approximated by using a quadrature formula with m nodes as follows,

$$E\left\{g^k\right\} = \int_{-\infty}^{\infty} \left[g\left(x\right)\right]^k \phi\left(x\right) \mathrm{d}x \cong \sum_{i=1}^{m} w_i \left[g\left(l_i\right)\right]^k \qquad (1)$$

where l_i and w_i denote the i-th quadrature node, i.e., the level, and the corresponding weight, respectively and $\phi(x)$ is the PDF of x. With m quadrature nodes, up to $(2m-1)$-th order polynomial function can be integrated exactly and therefore at least three nodes are necessary to obtain the first four moments required by the Pearson system. As shown in Fig. 1, levels and their corresponding weights for three-level design of experiment (DoE) are suggested by Taguchi (1978) for uniform distribution, by D'Errico and Zaino (1988) for normal distribution, and by Seo and Kwak (2002) for non-normal distribution, respectively.

However, for the higher levels above three, it is impossible to determine analytically the levels and weights of non-normal distribution. Therefore, to improve the accuracy of moments, Zhao and Ono (2000) proposed five and seven integration nodes numerically in standard normal space and Rahman and Xu (2004)

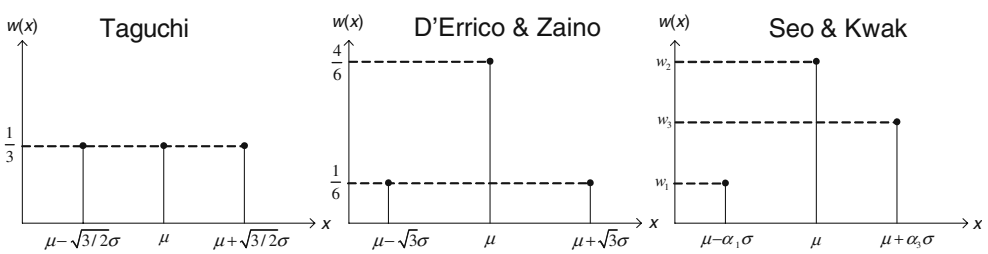

Fig. 1 Levels and weights for three-level DoE

and Xu and Rahman (2005) proposed a method to determine the general levels and weights for non-normal distribution, which is called MBQR. Lee et al. (2008) also proposed a multi-level DoE to determine levels and weights. In MBQR, a system of linear equations should be solved to determine the integration nodes. However, for the case of many integration nodes or small coefficient of variance of random variable, the system of linear equations as shown in (2) may be ill-posed, which degrades the accuracy of the levels and weights. To avoid this, Ju and Lee (2007) proposed an improved MBQR (IMBQR) in which the condition number of the matrix of linear equations is controlled.

The system of the linear equations to determine the levels and weights in MBQR is as follows,

$$\begin{bmatrix} \mu'_{m-1} & -\mu'_{m-2} & \cdots & (-1)^{m-1}\mu'_0 \\ \mu'_m & -\mu'_{m-1} & \cdots & (-1)^{m-1}\mu'_1 \\ \vdots & \vdots & \vdots & \vdots \\ \mu'_{2m-2} & -\mu'_{2m-3} & \cdots & (-1)^{m-1}\mu'_{m-1} \end{bmatrix} \begin{bmatrix} r_1 \\ r_2 \\ \vdots \\ r_m \end{bmatrix} = \begin{bmatrix} \mu'_m \\ \mu'_{m+2} \\ \vdots \\ \mu'_{2m-1} \end{bmatrix} \tag{2}$$

where μ'_i denotes the i-th raw moment of random variable, x, and r_i denotes the coefficient of polynomial equation defined in (3) below.

After solving for r_i from (2), the integration nodes l_i, $i = 1, ..., m$ can then be obtained as the i-th root of the following equation.

$$x^m - r_1 x^{m-1} + r_2 x^{m-2} - ... + (-1)^m r_m = 0$$

$$\text{where } r_1 = \sum_{i=1}^{m} l_i,$$

$$r_2 = \sum_{i=1}^{m}\sum_{j=i+1}^{m} l_i l_j, ..., r_m = l_1 l_2 ... l_m \tag{3}$$

And their corresponding weights are determined from the following equation.

$$w_i = \frac{\int_{-\infty}^{\infty} \prod_{k=1,k\neq i}^{m} (x - l_k)\phi(x)\,dx}{\prod_{k=1,k\neq i}^{m} (x_i - l_k)} = \frac{\sum_{k=0}^{m-1} (-1)^k \mu'_{m-k-1} q_{ik}}{\prod_{k=1,k\neq i}^{m} (x_i - l_k)} \tag{4}$$

where $q_{i0} = 1, q_{ik} = r_k - l_i q_{i(k-1)}$ and $\phi(x)$ is PDF of random variable, x.

After determining the m levels and weights for each independent random variable by MBQR, the k-th order raw moment can be calculated by m^n full factorial design from the product quadrature rule as follows:

$$E\{g^k\} = \int_{-\infty}^{\infty} \cdots \int_{-\infty}^{\infty} [g(x_1, \cdots x_n)]^k \prod_{i=1}^{n} \phi(x_i) dx_1 \cdots dx_n \cong \sum_{j_1=1}^{m} w_{1,j_1} \cdots \sum_{j_n=1}^{m} w_{n,j_n} \left[g\left(l_{1,j_1}, \cdots, l_{n,j_n}\right)\right]^k \tag{5}$$

where $l_{i,j}$ and $w_{i,j}$ and $\phi(x)$ denote the j-th level and weight of the i-th variable and PDF of random variable, x, respectively.

3 Maximum entropy principle

3.1 MEP formulation

It is well known that the PDF determined from a finite number of moments of a performance function is not a unique one which satisfies the given moment conditions and that the PDFs which satisfy the given moment conditions have some similarity with each other in their shapes as shown in Fig. 2 (Stuart and Ord 1994). MEP provides a means to determine the PDF which maximizes the entropy $H(p) = -\Sigma p_i \log p_i$ and satisfies the given moment conditions (Shannon 1948; Jaynes 1957). The maximization of entropy implies physically the minimization of spurious information of a system. Therefore, according to the information theory criterion, the PDF estimated based on MEP is the least biased estimate possible on the given partial moment information and, in other words, "it is maximally

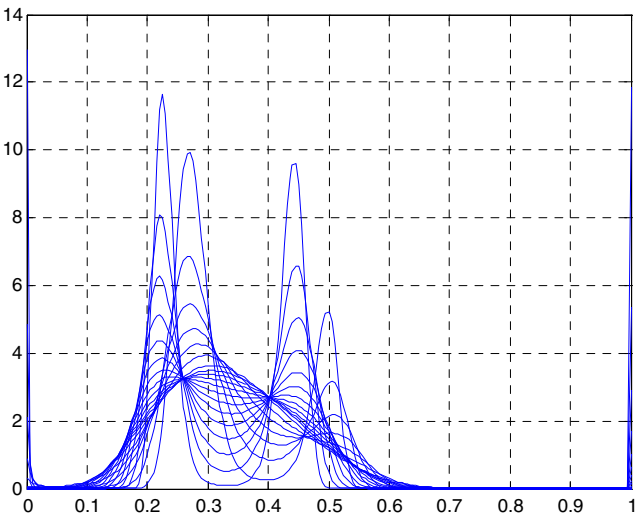

Fig. 2 Same the first four moments but different function shapes

noncommittal with regard to missing information" (Papoulis and Pillai 2002). In brief, The MEP gives the most probable PDF model among all PDF candidates which satisfy the given information

The MEP formulation subject to a given partial moment constraints for continuous PDF is as follows (Cover and Thomas 1991),

$$\begin{aligned} &\text{maximize} \int_a^b p(x)\log p(x)\,dx \\ &\text{subject to } p(x)\geq 0,\ \int_a^b p(x)\,dx = 1, \\ &\int_a^b x^i p(x)\,dx = \mu_i',\ \text{for } 1\leq i\leq nm \end{aligned} \tag{6}$$

where μ_i' is the i-th raw moment of random variable, nm denotes the number of given moment constraints and $p(x)$ denotes the PDF to be sought. By using the calculus of variation, the closed form solution of (6) is as follows,

$$p(x) = \exp\left[\sum_{i=0}^{nm}\lambda_i x^i\right],\ x\in[a,b] \tag{7}$$

where λ_i is the Lagrange multiplier and $(nm+1)$ Lagrange multipliers should be determined by the given $(nm+1)$ moment constraints.

The procedure to determine the Lagrange multipliers for given moment constraints is the same as the procedure to solve a system of nonlinear equations for $(nm+1)$ unknowns. It is, however, impossible to determine an analytical solution except for a special case (Mead and Papanicolaou 1984) and it is also difficult to find a numerical solution by conventional nonlinear system equation solver such as NEQNF (IMSL 2000) based on a modified Powell hybrid algorithm in IMSL library. Therefore, a potential function has been introduced as follows through the Legendre transformation to determine Lagrange multipliers indirectly (Mead and Papanicolaou 1984).

$$\begin{aligned} &\Gamma(\boldsymbol{\lambda}) = \ln Z + \sum_{i=1}^{nm}\mu_i'\lambda_i \text{ where} \\ &Z \equiv \int_a^b \exp\left(-\sum_{i=1}^{nm}\lambda_i x^i\right)\mathrm{d}x \end{aligned} \tag{8}$$

A stationary point of $\Gamma(\boldsymbol{\lambda})$ is the Lagrange multipliers which satisfy the given moment constraints because $\Gamma(\boldsymbol{\lambda})$ is everywhere convex and the Hessian of $\Gamma(\boldsymbol{\lambda})$, which is obtained as (9), is positive definite,

$$H_{ij} = \frac{\partial^2\Gamma}{\partial\lambda_i\partial\lambda_j} = \langle x^{i+j}\rangle - \langle x^i\rangle\langle x^j\rangle \tag{9}$$

where $\langle x^n\rangle$ denotes the expected value of x^n.

Another form of potential function is also defined by introducing Lagrange multiplier λ_0 as follows,

$$\Delta(\boldsymbol{\lambda}) = \int_a^b \exp\left(-\sum_{i=0}^{nm}\lambda_i x^i - 1\right)\mathrm{d}x + \sum_{i=0}^{nm}\lambda_i\mu_i' \tag{10}$$

This potential function $\Delta(\boldsymbol{\lambda})$ is also convex and its Hessian matrix is positive definite.

The stationary points of the potential function are the Lagrange multipliers of (7). The procedure to find the stationary point of $\Gamma(\boldsymbol{\lambda})$ is the same as that of solving the following nonlinear system of equations,

$$\begin{aligned} &\frac{\partial\Gamma}{\partial\lambda_n} = \frac{1}{Z}\frac{\partial Z}{\partial\lambda_n} + \mu_n' = 0,\ n = 1,..,nm \\ &\qquad -\langle x^n\rangle + \mu_n' = 0,\ n = 1,...,nm \text{ where} \\ &\langle x^n\rangle \equiv \frac{\int_a^b x^n\exp\left(-\sum_{i=1}^{nm}\lambda_i x^i\right)\mathrm{d}x}{\int_a^b \exp\left(-\sum_{i=1}^{nm}\lambda_i x^i\right)\mathrm{d}x} \end{aligned} \tag{11}$$

Due to the properties of $\Gamma(\boldsymbol{\lambda})$, the convexity and the positive definiteness of its Hessian matrix, the stationary point can be determined by an iterative Newton algorithm. The iterative scheme for finding the Lagrange multipliers is shown in (12) below. The updating procedure is initialized setting all the Lagrange multipliers equal to zero and $\langle x^n\rangle^k$ denotes the expected value of x^n at the k-th iteration step and should be normalized by Z, which is defined in (8).

$$\begin{aligned} \lambda_i^{k+1} &= \lambda_i^k - \sum_{j=1}^{nm}\left(H^{-1}\right)_{ij}^k\frac{\partial\Gamma}{\partial\lambda_j^k} \\ &= \lambda_i^k - \sum_{j=1}^{nm}\left(H^{-1}\right)_{ij}^k\left[\mu_j' - \langle x^j\rangle^k\right] \\ \text{where } H_{ij}^k &= \frac{\partial^2\Gamma}{\partial\lambda_i\partial\lambda_j} = \langle x^{i+j}\rangle^k - \langle x^i\rangle^k\langle x^j\rangle^k\, i, \\ &\qquad j = 1,2,...,nm \end{aligned} \tag{12}$$

The overall procedure to determine the Lagrange multipliers for potential function $\Delta(\boldsymbol{\lambda})$ is similar to that of $\Gamma(\boldsymbol{\lambda})$ and the nonlinear system of equations for $\Delta(\boldsymbol{\lambda})$ are as follows,

$$\begin{aligned} &\frac{\partial\Delta}{\partial\lambda_n} = -\int_a^b x^n\exp\left(-\sum_{i=0}^{nm}\lambda_i x^i\right)\mathrm{d}x + \mu_n' = 0, \\ &n = 0,1,...nm - \langle x^n\rangle + \mu_n' = 0, n = 0,1,...nm \\ &\qquad \text{where } \langle x^n\rangle \equiv \int_a^b x^n\exp\left(-\sum_{i=0}^{nm}\lambda_i x^i\right)\mathrm{d}x \end{aligned} \tag{13}$$

Table 1 Raw moments of Gumbel distribution [$a = 0.3, b = 0.06$]

1st	2nd	3rd	4th	5th	6th	7th
3.34633×10^{-1}	1.17901×10^{-1}	4.39361×10^{-2}	1.74025×10^{-2}	7.36351×10^{-3}	3.34480×10^{-3}	1.63811×10^{-3}

The iteration scheme for $\Delta(\boldsymbol{\lambda})$ is also as follows,

$$\begin{aligned}\lambda_i^{k+1} &= \lambda_i^k - \sum_{j=0}^{nm} \left(H^{-1}\right)_{ij}^k \frac{\partial \Delta}{\partial \lambda_j^k} \\ &= \lambda_i^k - \sum_{j=0}^{nm} \left(H^{-1}\right)_{ij}^k \left[\mu_j' - \langle x^j \rangle^k\right] \\ \text{where } H_{ij}^k &= \frac{\partial^2 \Delta}{\partial \lambda_i \partial \lambda_j} = \langle x^{i+j} \rangle^k \, i, \\ & j = 0, 1, 2, \ldots, nm \end{aligned} \tag{14}$$

The Hessian matrix of potential function $\Delta(\boldsymbol{\lambda})$ is $(nm+1) \times (nm+1)$ matrix and its inverse matrix always exists because of its positive definiteness. For the PDF modeling for reliability analysis and RBDO examples, the potential function $\Delta(\boldsymbol{\lambda})$ is used in this study because the normalization of $\langle x^n \rangle$ in (11), which is a cause of numerical instability at the boundary of moment space, is not necessary. Furthermore, $\Delta(\boldsymbol{\lambda})$ is not a rational function of $\boldsymbol{\lambda}$ like $\Gamma(\boldsymbol{\lambda})$ but a polynomial function of $\boldsymbol{\lambda}$**.** Therefore, it is easy to derive the derivatives of the Langrage multipliers with respect to moments for the sensitivity analysis.

The positive definiteness of the Hessian matrix of $\Delta(\boldsymbol{\lambda})$ is the same as one of the Hankel determinant conditions which guarantee the existence of a PDF for a given set of moments (Athanassoulis and Gavriliadis 2002). To apply the Hankel determinant conditions for a given set of moments, the given moments need be reduced to within a unit range [0,1] and therefore the supporting range $[a,b]$ of PDF for random variable x should be transformed to [0,1] and the relationship between random variable x and normalized variable z is as follows:

$$z = \frac{x - a}{b - a} \tag{15}$$

The relationship between the raw moment of x and the raw moment of z is as follows:

$$\begin{aligned}\mu_{z,i}' &= \int_0^1 z^i f(z)\,\mathrm{d}z = \int_a^b \left(x - a/b - a\right)^i f(x)\,\mathrm{d}x \\ &= \frac{1}{(b-a)^i} \sum_{j=0}^{i} \binom{i}{j} (-a)^j \int_a^b x^{i-j} f(x)\,\mathrm{d}x \\ &= \frac{1}{(b-a)^i} \sum_{j=0}^{i} \binom{i}{j} (-a)^j \mu_{x,i-j}' \end{aligned} \tag{16}$$

$$\begin{aligned}\mu_{x,i}' &= \int_a^b x^i f(x)\,\mathrm{d}x = \int_0^1 (a + (b-a)\,z)^i \, f(z)\,\mathrm{d}z \\ &= \sum_{j=0}^{i} \binom{i}{j} a^{i-j} (b-a)^j \int_0^1 z^i f(z)\,\mathrm{d}z \\ &= \sum_{j=0}^{i} \binom{i}{j} a^{i-j} (b-a)^j \mu_{z,j}' \end{aligned} \tag{17}$$

where $\mu_{x,i}'$ and $\mu_{z,i}'$ are the i-th order raw moment of random variable x and z, respectively.

3.2 Verification examples

3.2.1 Reconstruction of Gumbel distribution

The first example is to examine the performance of the MEP as compared with the Pearson system by considering a reconstruction of a Gumbel distribution from a given finite number of moments. The PDF of a test Gumbel distribution is defined as follows,

$$f(x) = \exp\left[(a-x)/b - \exp\left[(a-x)/b\right]\right]/b \tag{18}$$

The parameters a and b are 0.3 and 0.06, respectively and the first seven moments that are obtained by numerical integration of (18), are shown in Table 1.

The estimated PDFs from the MEP (using 4, 5, 6 and 7 moments) and the Pearson system are compared with the original PDF and the error defined as (19) is summarized in Table 2.

$$\text{Error} = \int_a^b \left| p_{\text{org}}(x) - p_{\text{app}}(x) \right| \mathrm{d}x \tag{19}$$

where p_{org} and p_{app} denote a original PDF and an approximated PDF by each method, respectively.

In this example, it is observed that including higher order moments decreases the error between the original PDF and the approximated one as shown in Table 2. In the following, MEP-k denotes the MEP using the first k moments. For the case of MEP-4, although the

Table 2 Error and entropy of each method for Gumbel distribution

Method	Error	Entropy
MEP-4 moments	0.057865	−1.231261
MEP-5 moments	0.038406	−1.234128
MEP-6 moments	0.013718	−1.235820
MEP-7 moments	0.008994	−1.235891
Pearson system	0.017653	−1.239820

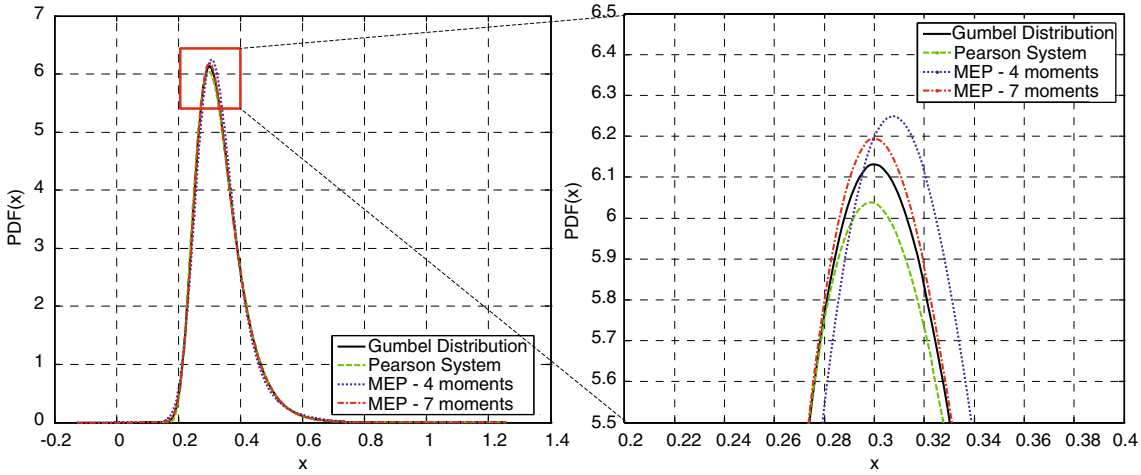

Fig. 3 Comparison of PDF estimated by MEP and Pearson system for Gumbel distribution

entropy of the Pearson system is less than that of MEP-4 and both method use the same number of moments, the error by the Pearson system is less than the error by the MEP-4. An important observation follows. It is obvious that the MEP method should recover the original PDF as the number of moments approaches infinity, if no round-off errors are involved. However for a given finite number of moments, for example, with four moments, it is the case that either the MEP or the Pearson system recovers the original better than the other because only partial information is used. In the above case, the fact that the Pearson system has given more similar PDF to the original PDF does not guarantee anything and accuracy has no meaning in reconstructing a PDF. The error defined is simply a measure of the difference between the partial and the whole information.

Figure 3 shows the estimated PDF by the MEP and the Pearson system. The overall shapes of the PDF resemble each other but there exist slight differences around the mode as shown in Fig. 3. The supporting range for the MEP is decided as $[\mu - 6\sigma, \mu + 12\sigma]$ in this example.

3.3 Reconstruction of bimodal distribution

To explain the flexibility of the proposed approach, a bimodal PDF is adopted as a second example. Equation (20) is the mixed form of Beta distribution and therefore it has dual mode,

$$f(x) = \frac{(x-a)^{q-1}(b-x)^{r-1} + (x-a)^{r-1}(b-x)^{q-1}}{2\text{Beta}(q,r)(b-a)^{q+r-1}} \tag{20}$$

The parameters taken are $(a, b) = (-1, 1)$ and $(q, r) = (24, 12)$, and the first eight raw moments of (20) are shown in Table 3. The resemblance of estimated PDF is compared based on (19) as in the first example. It is observed that including higher moments reduce the error between the original and the estimated PDF as shown in Table 4. In this example, the PDF by the Pearson system as shown in Fig. 4 is not dual but single mode. From this example, it is seen that not only the error decreases by accommodating higher moments as in the first example but also it is flexible enough to recover a dual mode PDF.

3.3.1 Fortini's clutch

The third example is the overrunning clutch assembly known as Fortini's clutch (Lee and Kwak 2006). The contact angle y in Fig. 5 is determined by the independent random variable, x_1, x_2, x_3 and x_4 as follows,

$$y = \arccos\left[2x_1 + (x_2 + x_3)/2x_4 - (x_2 + x_3)\right] \tag{21}$$

Table 3 Raw moments of bimodal distribution $[a = -1, b = 1, q = 24, r = 12]$

1st	2nd	3rd	4th	5th	6th	7th	8th
0.000000	1.35135×10^{-1}	0.000000	2.89237×10^{-2}	0.000000	7.82940×10^{-3}	0.000000	2.48483×10^{-3}

Table 4 Error and entropy of each method for bimodal distribution

Method	Error	Entropy
MEP-4 moments	0.137718	0.203027
MEP-6 moments	0.095519	0.195235
MEP-8 moments	0.047616	0.189842
Pearson system	N/A	N/A

The distribution parameters of random variables are listed in Table 5. The moments of a performance function evaluated by five-level MBQR are compared with MCS results to check the accuracy of the moment estimation in Table 6. The Pearson system and MEP use these moments calculated by MBQR to determine the PDF of the contact angle y. The cumulative densities of the contact angle by each method and the entropies for each PDF model are listed in Table 7. In this example, the true PDF of the contact angle is unknown and therefore the MCS result is adopted as a reference PDF. However, the MCS result also has variations and therefore it is checked whether the estimated probability falls in the confidence interval, which is defined as follows (Hahn and Shapiro 1968),

$$p' - E \le p \le p' + E \text{ where } E^2 = \frac{p'\left(1-p'\right)}{n'} z^2_{1-\alpha/2} \tag{22}$$

where n', p' and p are the number of experiments for the Monte Carlo simulation (MCS), the estimated failure probability and the true failure probability, respectively. The subscript $1–\alpha$ denotes the confidence

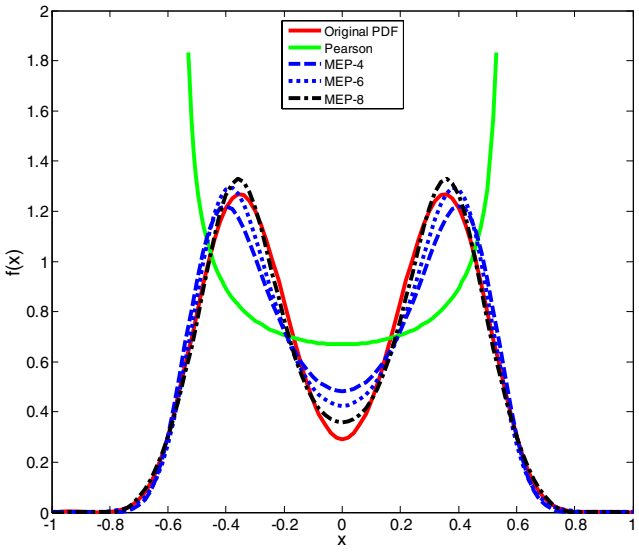

Fig. 4 Comparison of PDF estimated by MEP and Pearson system for bimodal distribution

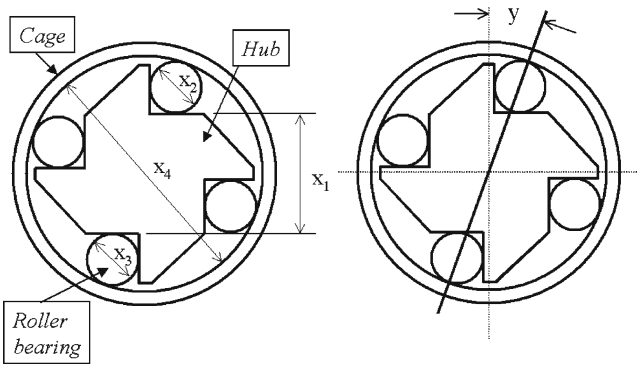

Fig. 5 Overrunning clutch assembly

level and for 1 - α = 95% confidence level, z is 1.96 as can be verified from the standard normal distribution table. The estimated PDFs by each method are shown in Fig. 6. In Fig. 7, the lower and upper bound of confidence interval for each case are normalized into 0 and 1, and the existence of an estimated probability in the confidence bound is checked. Although all PDFs are similar each other graphically in Fig. 6, as shown in Fig. 7, the probability by the Pearson system exists out of the confidence bound, which means that the estimated probability does not coincide with the real one. However, the probability by the MEP (except MEP-4 for Pr[y < 6] and Pr[y < 9]) exists inside the confidence bound.

4 Sensitivity analysis

4.1 Formulation

The failure probability of a performance function is a function of its moments which are dependent on the design variables and defined as follows,

$$\begin{aligned}\Pr\left[g\left(x\right) < 0\right] &= \Pr\left(\boldsymbol{\mu}'\left(\mathbf{d}\right)\right) = \int_{g(x)<0} p\left(x\right) \mathrm{d}x \\ &= \int_a^0 \exp\left(-\sum\nolimits_{i=0}^{nm} \lambda_i x^i\right) \mathrm{d}x \\ &= \int_0^\alpha \exp\left(-\sum\nolimits_{i=0}^{nm} \lambda_i z^i\right) \mathrm{d}z \end{aligned} \tag{23}$$

Table 5 Random variables in Fortini's clutch

Variables	Mean [mm]	STD [mm]	Dist. type	Parameters
x_1	55.29	0.0793	Beta	$q = r = 5.0$
x_2	22.86	0.0043	Normal	
x_3	22.86	0.0043	Normal	
x_4	101.60	0.0793	Rayleigh	$101.45 \le x_4$, $s = 0.1211$

Table 6 Raw moment of Fortini's clutch

	1st $\times 10^{-1}$	2nd $\times 10^{-2}$	3rd $\times 10^{-3}$	4th $\times 10^{-4}$	5th $\times 10^{-5}$	6th $\times 10^{-6}$
Five-level	1.21930	1.50034	1.86258	2.33217	2.94447	3.74752
MCS[a]	1.21930	1.50034	1.86258	2.33217	2.94471	3.74752

[a]Number of experiments for MCS = 10^6

where **d**, a, nm and z denote the design variable vector, the lower bound of the PDF supporting range in the original range, the number of moments used to estimate the PDF and the random variable reduced in the unit range, respectively. A value α in the unit range [0,1] corresponds to zero in the original range [a,b].

The derivative of the failure probability with respect to the i-th design variable can be written as follows using chain rule.

$$\frac{\partial \Pr}{\partial d_i} = \sum_{k=0}^{nm} \frac{\partial \Pr}{\partial \lambda_k} \sum_{j=0}^{nm} \frac{\partial \lambda_k}{\partial \mu'_j} \frac{\partial \mu'_j}{\partial d_i}$$

$$\text{where } \Pr = \int_0^{\alpha} p(z)\, dz = \int_0^{\alpha} \exp\left(\sum_{i=0}^{nm} -\lambda_i z^i\right) dz \tag{24}$$

$\partial \Pr/\partial \lambda_k$ in (24) can be calculated from the PDF estimated by MEP as follows,

$$\frac{\partial \Pr}{\partial \lambda_k} = -\int_0^{\alpha} z^k \exp\left(\sum_{i=0}^{nm} -\lambda_i z^i\right) dz \tag{25}$$

However, a direct derivation of $\partial \lambda_k / \partial \mu'_j$ is difficult and therefore the relations between the estimated PDF and the normalized raw moment are used to derive the derivatives. Differentiation of both sides of (26) with respect to the j-th order normalized raw moment yields (27) and (28) as,

$$\int_0^1 z^n \exp\left(-\sum_{i=0}^{nm} \lambda_i z^i\right) \mathrm{d}z = \mu'_n,\ n = 0, 1, \ldots nm \tag{26}$$

$$\begin{aligned} &\frac{\partial}{\partial \mu'_j} \int_0^1 z^n \exp\left(-\sum_{i=0}^{nm} \lambda_i z^i\right) \mathrm{d}z \\ &\quad = \int_0^1 -z^{n+k} \exp\left(-\sum_{i=0}^{nm} \lambda_i z^i\right) \mathrm{d}z \sum_{k=0}^{nm} \frac{\partial \lambda_k}{\partial \mu'_j} \\ &\quad = -\mu'_{n+k} \sum_{k=0}^{nm} \frac{\partial \lambda_k}{\partial \mu'_j},\ n,\ j = 0, 1, \ldots nm \end{aligned} \tag{27}$$

$$\frac{\partial \mu'_n}{\partial \mu'_n} = \delta_{nj},\ n,\ j = 0, 1, \ldots nm \tag{28}$$

The system of linear equations given by (26), (27) and (28) can be rearranged in a matrix form as follows,

$$\begin{bmatrix} \mu'_0 & \mu'_1 & \cdots & \mu'_{nm} \\ \mu'_1 & \mu'_2 & \cdots & \mu'_{nm+1} \\ \vdots & \vdots & \ddots & \vdots \\ \mu'_{nm} & \mu'_{nm+1} & \cdots & \mu'_{2nm} \end{bmatrix} \begin{bmatrix} \partial\lambda_0/\partial\mu'_0 & \partial\lambda_0/\partial\mu'_1 & \cdots & \partial\lambda_0/\partial\mu'_{nm} \\ \partial\lambda_1/\partial\mu'_0 & \partial\lambda_1/\partial\mu'_1 & \cdots & \partial\lambda_1/\partial\mu'_{nm} \\ \vdots & \vdots & \ddots & \vdots \\ \partial\lambda_{nm}/\partial\mu'_0 & \partial\lambda_{nm}/\partial\mu'_1 & \cdots & \partial\lambda_{nm}/\partial\mu'_{nm} \end{bmatrix} = \begin{bmatrix} -1 & 0 & \cdots & 0 \\ 0 & -1 & \cdots & 0 \\ \vdots & \vdots & \ddots & \vdots \\ 0 & 0 & \cdots & -1 \end{bmatrix} \tag{29}$$

Table 7 Cumulative density of Fortini's clutch

	MCS	MEP-4	MEP-5	MEP-6	Pearson
$\Pr[y < 5°]$	0.001288	0.001376	0.001237	0.001193	0.001396
$\Pr[y < 6°]$	0.073922	.072832	0.073530	0.073672	0.072715
$\Pr[y < 7°]$	0.503160	0.504265	0.503126	0.503144	0.504525
$\Pr[y < 8°]$	0.936726	0.936147	0.936793	0.936631	0.935948
$\Pr[y < 9°]$	0.999190	0.999306	0.999192	0.999227	0.999345
Entropy		−3.03111	−3.03116	−3.03117	−3.03112

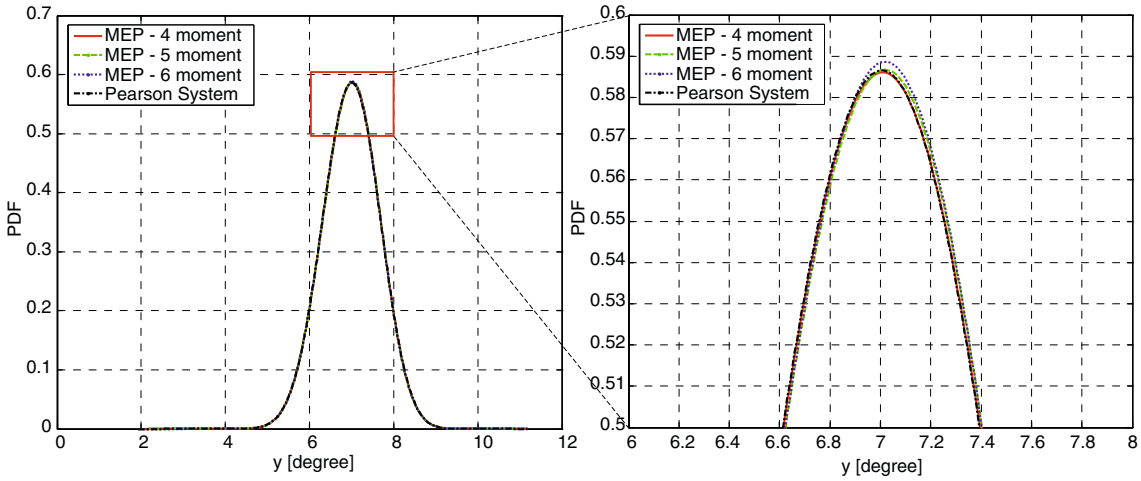

Fig. 6 Comparison of PDF estimated by MEP and Pearson system for Fortini's clutch

After solving (29), the derivative of the Lagrange multiplier with respect to the normalized raw moment is calculated as follows,

$$\frac{\partial \lambda_i}{\partial \mu'_j} = -C_{ji} \text{ where } \mathbf{C} = \mathbf{A}^{-1} = \begin{bmatrix} \mu'_0 & \mu'_1 & \cdots & \mu'_{nm} \\ \mu'_1 & \mu'_2 & \cdots & \mu'_{nm+1} \\ \vdots & \vdots & \ddots & \vdots \\ \mu'_{nm} & \mu'_{nm+1} & \cdots & \mu'_{2nm} \end{bmatrix}^{-1} \tag{30}$$

The derivative of the j-th order normalized raw moment with respect to the i-th design variable is obtained by using FDM as follows,

$$\frac{\partial \mu'_j}{\partial d_i} \cong \frac{\Delta \mu'_j}{\Delta d_i} \tag{31}$$

The above equations are summarized as follows,

$$\frac{\partial \Pr}{\partial d_i} = \sum_{k=0}^{nm} \frac{\partial \Pr}{\partial \lambda_k} \sum_{j=0}^{nm} \frac{\partial \lambda_k}{\partial \mu'_j} \frac{\partial \mu'_j}{\partial d_i}$$

$$\text{where } \Pr = \int_0^{\alpha} p(z)\,\mathrm{d}z = \int_0^{\alpha} \exp\left(\sum_{i=0}^{nm} -\lambda_i z^i\right) \mathrm{d}z$$

$$\frac{\partial \Pr}{\partial \lambda_k} = -\int_0^{\alpha} z^k \exp\left(\sum_{i=0}^{nm} -\lambda_i z^i\right) \mathrm{d}z\,,$$

$$\frac{\partial \lambda_k}{\partial \mu'_j} = -C_{jk}\,, \quad \frac{\partial \mu'_j}{\partial d_i} \cong \frac{\Delta \mu'_j}{\Delta d_i} \tag{32}$$

4.2 Verification

Numerical examples are taken from RBDO example of Tu et al. (2001) to verify the accuracy of the derived sensitivity formulation and the results are compared with the sensitivity obtained by FDM. The first four moments are used and the moments of each performance function are obtained by five-level MBQR. The sensitivities are compared at three design points, which are iteration points during the optimization. The first performance function is a polynomial of random variables, $x_1 \sim N(\mu_1,0.5)$ and $x_2 \sim N(\mu_2,0.4)$,

$$\Pr\left[g_1 \le 0\right] \text{ where } g_1 = \frac{x_1^2 x_2}{20} - 1 \tag{33}$$

The results are summarized in Table 8. The derived formula and the FDM give almost the same results with less than 0.12% difference. For the FDM, a forward

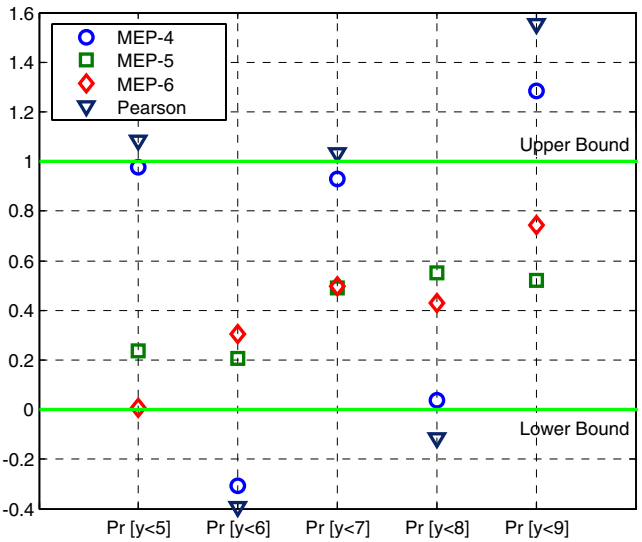

Fig. 7 Lower and upper bound of 99% confidence level and failure probability by each method

Table 8 Comparison of sensitivity of a performance function 1

Design point	Derived formulation		FDM[a]		Difference [%]	
	x_1	x_2	x_1	x_2	x_1	x_2
(4.000, 4.000)	-3.431×10^{-3}	-1.132×10^{-3}	-3.427×10^{-3}	-1.132×10^{-3}	−0.12	−0.04
(3.500, 3.500)	-8.029×10^{-2}	-3.160×10^{-2}	-8.022×10^{-2}	-3.159×10^{-2}	−0.09	−0.03
(3.968, 2.540)	-8.536×10^{-2}	-6.434×10^{-2}	-8.529×10^{-2}	-6.431×10^{-2}	−0.07	−0.05

[a]Finite difference size $= 0.001 \times \sigma$

Table 9 Comparison of sensitivity of a performance function 2

Design point	Derived formulation		FDM[a]		Difference [%]	
	x_1	x_2	x_1	x_2	x_1	x_2
(4.000, 4.000)	3.564×10^{-5}	2.217×10^{-5}	3.569×10^{-5}	2.195×10^{-5}	0.13	−1.03
(3.500, 3.500)	6.581×10^{-8}	3.546×10^{-8}	6.749×10^{-8}	3.249×10^{-8}	−2.56	−8.34
(3.968, 2.540)	8.377×10^{-8}	2.645×10^{-8}	8.390×10^{-8}	2.522×10^{-8}	0.15	−4.63

[a]Finite difference size $= 0.001 \times \sigma$

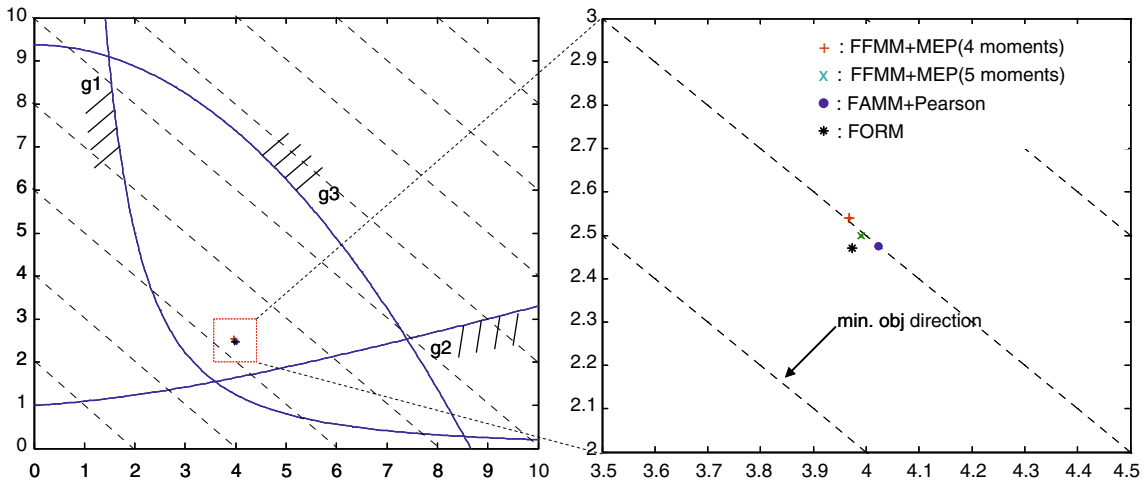

Fig. 8 Comparison of optimal point of each method for numerical example

Table 10 Optimization result of numerical example

$p_{f0} = 0.02275$	x_1	x_2	Objective value	Remarks
FORM[a]	3.974	2.470	6.444	HL-RF algorithm
FAMM + Pearson[a]	4.023	2.476	6.530	Three-level MBQR
FFMM + Pearson	4.004	2.480	6.484	Five-level MBQR 47(483)[b]
FFMM + MEP-4	3.968	2.540	6.508	Five-level MBQR 38(412)[b]
FFMM + MEP-5	3.990	2.500	6.485	Five-level MBQR 14(75)[b]

[a]Optimization results are taken from Huh (2006)
[b]Iteration (function calls)

Table 11 Constraint verification by MCS at optimal point for numerical example

$p_{f0} = 0.02275$	g_1	g_2	g_3
FORM	0.026340	0.023320	0.000000
FAMM + Pearson	0.021640	0.023660	0.000000
FFMM + Pearson	0.022849	0.022800	0.000000
FFMM + MEP-4	0.021500	0.015200	0.000000
FFMM + MEP-5	0.023000	0.020565	0.000000

g_1 and g_2 are active constraints; number of experiment for MCS = 10^6

difference is used with an increment of 0.1% of standard deviation.

The second performance function is shown below and the properties of random variables are the same as those of the first case,

$$\Pr\left[g_3 \le 0\right] \text{ where } g_3 = \frac{80}{\left(x_1^2 + 8x_2 + 5\right)} - 1 \tag{34}$$

The results are compared with the FDM results as listed in Table 9. An acceptable level of differences is shown at the first design point with less than 1% but a large difference by more than 1% is shown at the second and third design point. These points, however, are located rather far from the failure surface as shown in Fig. 8, where the failure probability is nearly zero.

5 RBDO examples

5.1 Numerical examples

The accuracy of the sensitivity by MEP is studied using numerical examples. Two RBDO problems are also solved by using the derived sensitivity formulation. The optimization results, by MEP-4 and MEP-5, are compared with those obtained by other reliability analysis method such as FORM and FAMM. The Pearson system is used as the PDF modeling method in FAMM.

The first example is taken from Tu et al. (2001), often cited when comparing RBDO algorithms. The problem with design variables $\mathbf{d} = [d_1,d_2]^T = [\mu_1, \mu_2]$ is defined as follows,

$$\begin{aligned}
&\text{minimize } f(d) = d_1 + d_2 \\
&\text{subject to } \Pr\left[g_i(\mathbf{x}) \le 0\right] \le p_f, i = 1, 2, 3 \\
&\qquad 0 \le \mathbf{d} \le 10 \\
&\text{where } g_1 = \frac{x_1^2 x_2}{20} - 1\,,\; g_2 = \frac{\left(10x_2^3 - x_1^2 x_2 - 2x_1\right)}{10} - 1\,, \\
&\qquad g_3 = \frac{80}{\left(x_1^2 + 8x_2 + 5\right)} - 1
\end{aligned} \tag{35}$$

The initial design point is $d_0 = [4.0,4.0]^T$ and statistical properties of random variables are $x_1 \sim N(d_1,0.5)$ and $x_2 \sim N(d_2,0.4)$. The target failure probability taken is $p_f = 0.02275$. The moments are evaluated using five-level MBQR and the optimization algorithm used is SQP. The results are summarized in Table 10. It is seen that the prescribed probabilistic constraints are satisfied when evaluated by MCS at each optimal point as shown Table 11. The 99% confidence interval of MCS result and the lower and upper bounds for each case are shown in Fig. 10, where pearson1 and pearson2 denote FFMM + Pearson system and FAMM + Pearson system, respectively.

FORM gives the lowest minimum among the five methods as listed in Table 10 but the constraint verification by MCS at the optimal point in Fig. 10 shows that all active constraints violate the probability constraints.

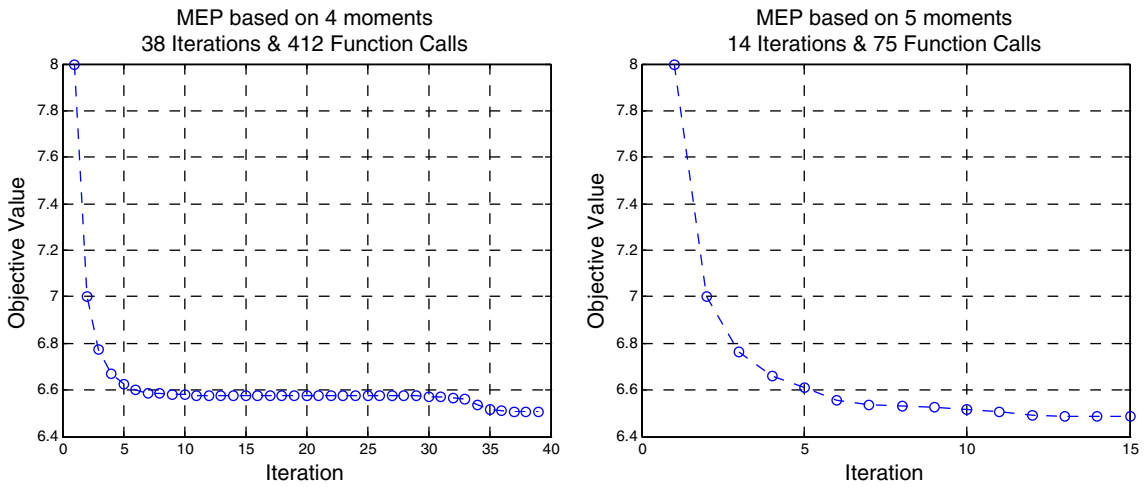

Fig. 9 History of optimization for numerical example

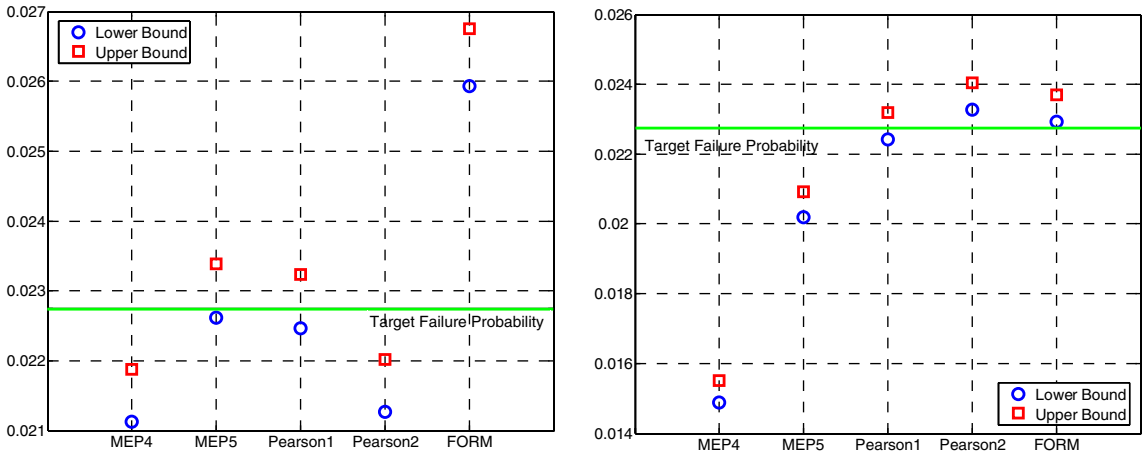

Fig. 10 MCS verification of active constraints with 99% confidence level

Table 12 Random variables in ONERA M6 wing

Variables	Mean	STD	Initial	PDF type	Var. bound
Mach #	0.84	0.003	0.84	Normal	[0.830, 0.850]
AoA	3.06	0.02	3.06	Normal	[3.015, 3.105]
Sweep angle	μ_{sweep}	0.10	30.26	Normal	[27.00, 45.00]
Taper ratio	μ_{taper}	0.02	0.56	Normal	[0.300, 0.600]

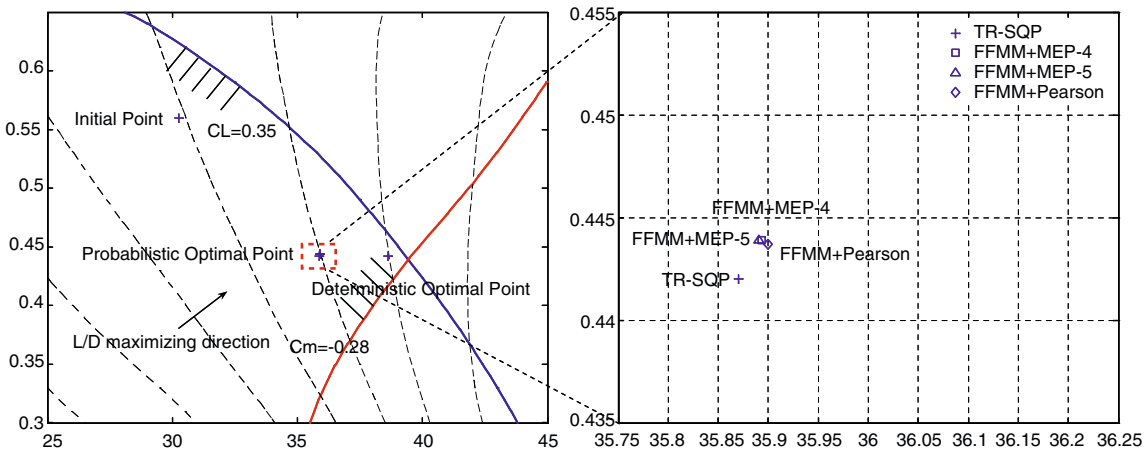

Fig. 11 Comparison of optimal point of each method for ONERA M6 wing

Table 13 Optimization result for OENRA M6 wing

	Sweep angle	Taper ratio	Obj.(L/D)	C_{L}	C_{m}	Remarks
Initial	30.2600	0.5600	19.6846	0.3620	−0.2265	
Deter. Opt.	38.63	0.4419	24.5748	0.3500	−0.2800	
TR-SQP[a]	35.87	0.4420	21.9438	0.3665	−0.2665	
FFMM + MEP-4	35.8936	0.4439	21.9773	0.3663	−0.2664	14(58)[b]
FFMM + MEP-5	35.8908	0.4439	21.9757	0.3663	−0.2664	15(61)[b]
FFMM + Pearson	35.8995	0.4437	21.9802	0.3663	−0.2664	36(373)[b]

[a]Optimization results are taken from Ahn and Kwon (2005)
[b]Iteration (function calls)

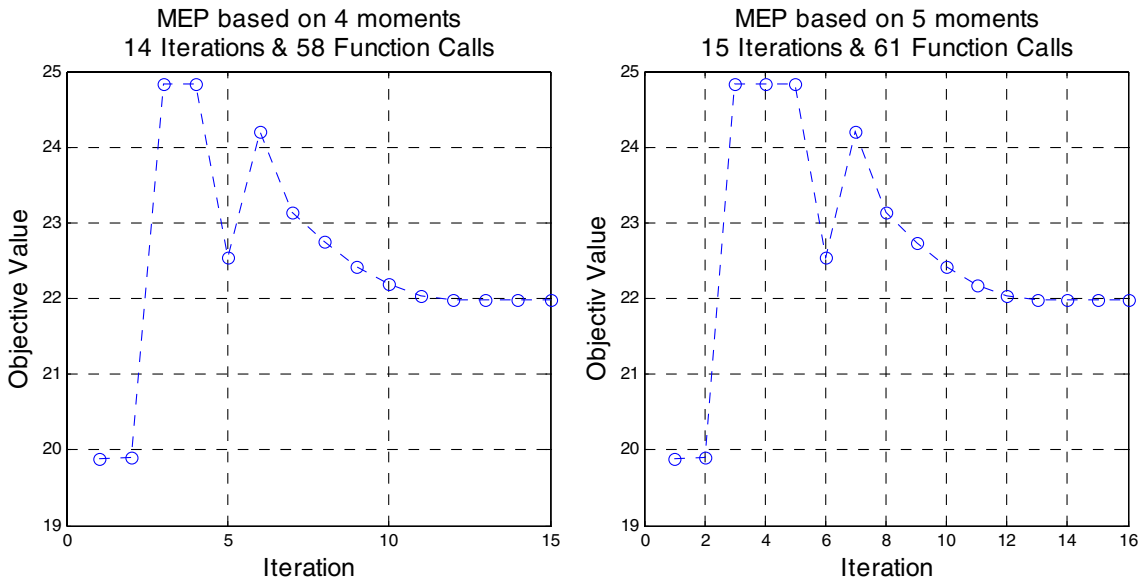

Fig. 12 History of optimization for ONERA M6 wing

The result obtained by FAMM + Pearson system also violates the active constraint g_2 as shown in Fig. 10. However, the result obtained by FFMM + MEP does satisfy constraints, and especially for the case of FFMM + MEP-5, the constraints are satisfied more tightly than FFMM + MEP-4 while improving the objective value: In fact, the constraints are not active, which means that there is a margin to improve the objective function. The optimal points are compared with each other in Fig. 8. In this example, compared with the MEP-based moment method, it is observed that the Pearson system-based method gives somewhat better result, but within the tolerance of stopping criteria. The Pearson system-based solution has constrains active, but there is still margin for them to become active in case of the MEP solution. The optimization histories for FFMM + MEP-4 and FFMM + MEP-5 are compared in Fig. 9. When five moments are used, the total number of iterations is reduced as shown in Fig. 9, showing a case that MEP-5 is more efficient than MEP-4 and the Pearson system. The amount of calculation for the moments at each iteration is the same for the Pearson system, the MEP-4 and MEP-5.

5.2 3-D wing optimization

The second RBDO example is taken from Ahn and Kwon (2005). A three-dimensional wing optimization under uncertainties is performed using the MEP-based moment method and the result is compared with other reliability analysis methods such as TR-SQP and the Pearson system-based moment method. The initial geometry of the wing is the ONERA M6 wing and the aerodynamic performances such as lift coefficient (C_{L}), pitching moment coefficient (C_{m}) and lift to drag ratio (L/D) are obtained by a compressible Euler code with an O–H type gird and $129 \times 33 \times 33$ grid points. The deliberated random variables are categorized into geometric random variables and operational random variables. The sweep angle and the taper ratio are geometric random variables and these are also design variables for optimization. The Mach number and the angle of attack are operational random variables. The statistical properties of the four random variables are listed in Table 12 and the initial design values are selected as those of OENRA M6 wing. A realistic RBDO formulation of the three-dimensional wing design is as follows,

$$\begin{aligned} &\text{maximize } L/D \\ &\text{subject to } \Pr[C_L \le 0.35] \le 0.00125 \\ &\qquad \Pr[C_m \le -0.28] \le 0.00125 \\ &\qquad 27 \le d_{\text{sweep}} \le 45,\ 0.3 \le d_{\text{taper}} \le 0.6 \end{aligned} \tag{36}$$

Table 14 Constraint verification by MCS at optimal point for ONERA M6 wing

	$\Pr[C_{\mathrm{L}} < 0.35]$	$\Pr[C_{\mathrm{m}} < -0.28]$
TR-SQP	0.000962	0.001368
FFMM + MEP-4	0.001234	0.001224
FFMM + MEP-5	0.001267	0.001294
FFMM + Pearson	0.001236	0.001331

Number of experiment for MCS = 10^6

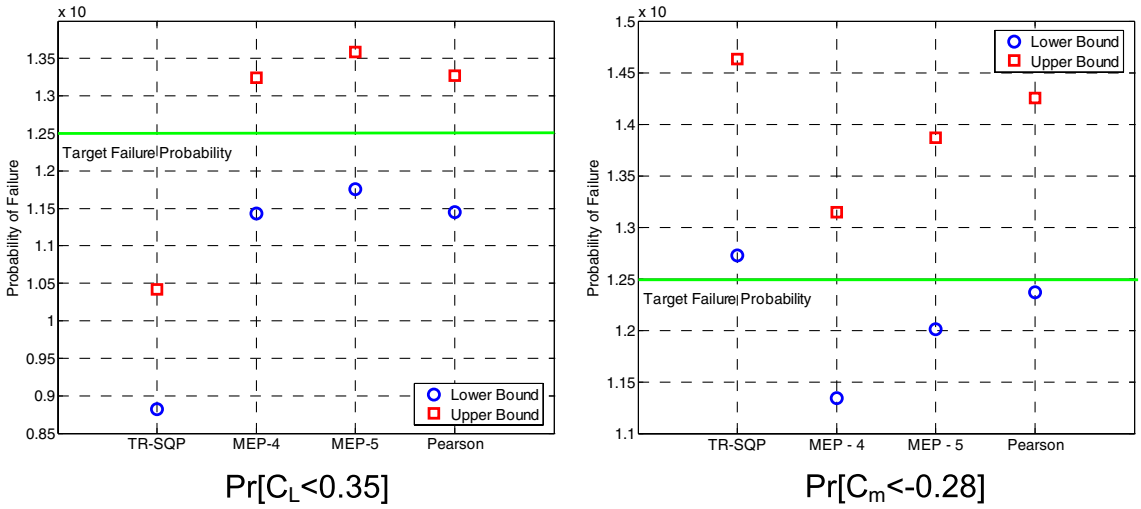

Fig. 13 MCS verification of active constraints with 99% confidence level

The lift to drag ratio, lift coefficient and pitching moment coefficient are evaluated by a regression model made by the Kriging method. A six-level full factorial experiment is used and therefore the total number of experiments to make the regression model is $6 \times 6 \times 6 \times 6 = 1{,}296$. Figure 11 shows the design space and the initial design values and the optimized design values for each method. The failure surfaces for lift coefficient and pitching moment coefficient are also shown in Fig. 11. The optimization results are summarized in Table 13. Among the three moment-based methods, the Pearson system-based moment method finds the largest objective value but it is observed that the total iteration is larger than the MEP-based moment methods. The objective value histories for MEP-4 and MEP-5 are shown in Fig. 12. Table 14 shows MCS verification of each constraint. The 99% confidence intervals of each constraint for each method are shown in Fig. 13. With respect to the accuracy, all methods except TR-SQP, which is based on FORM, satisfy more plausibly the probabilistic constraints as shown in Fig. 13. Also the MEP-based moment methods show higher efficiency than the Pearson system-based one as shown in Table 13. The optimized wing shapes and their pressure contours by each method are shown in Figs. 14 and 15. It is observed that the λ-shocks appear stronger for all

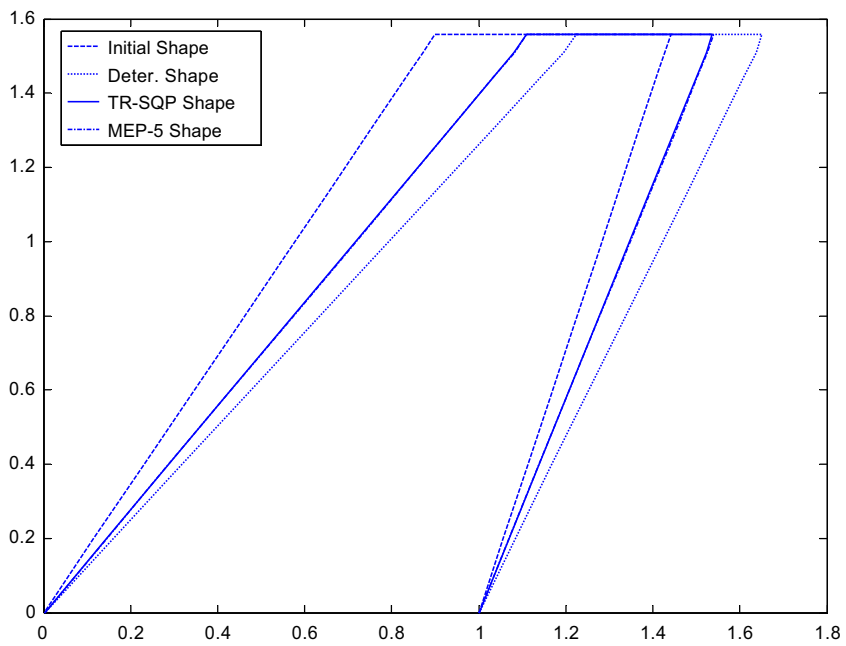

Fig. 14 Optimized wing shapes for ONERA M6 wing

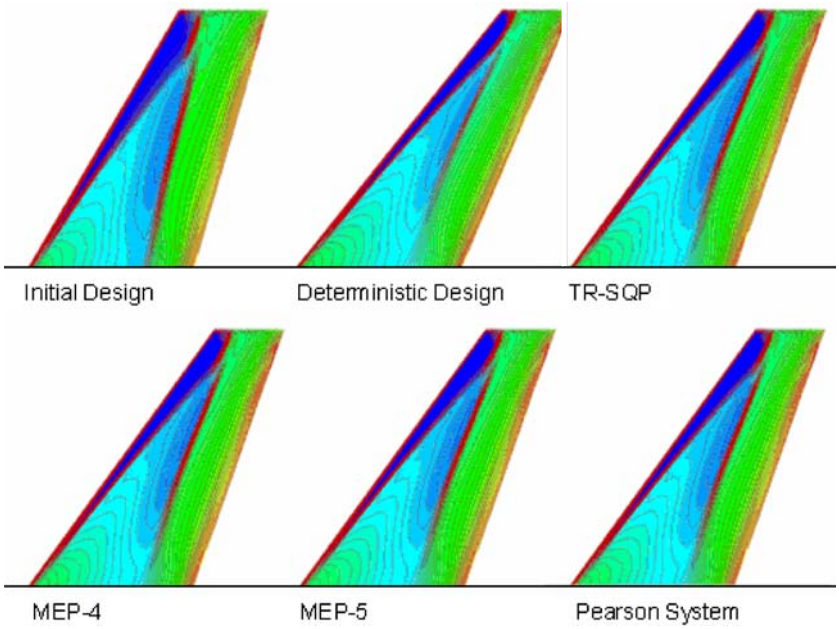

Fig. 15 Pressure contours for OENRA M6 wing

RBDO methods than the deterministic optimization as shown in Fig. 15 and therefore the λ-shocks need be considered in the design formulation with additional constraints as a further work.

6 Discussions and conclusions

The maximum entropy principle is first adopted for reliability calculation and reliability-based design and its performance is studied by several numerical examples including a three-dimensional wing design problem. It is found flexible enough of handling higher order moments, and efficient and accurate in obtaining RBDO solutions.

The possibility of allowing higher order moments in MEP formulation is a flexibility that the Pearson system does not have. Given more and more information a convergent solution is also expected. For a finite number of moments, the error introduced as a square error form denotes simply the gap between the partial information and the whole information case. Therefore this should not be interpreted as a measure of accuracy.

The Gumbel distribution example is such a case; under the same condition, i.e., using the first four moments, the Pearson system looks to give better PDF than the MEP-4 as far as reconstructing the given analytical distribution. This is not a matter of accuracy.

The sensitivity analysis of failure probability based on MEP is performed and applied to RBDO examples. The effect of higher order moments is studied through RBDO examples. For four moment case, it is not conclusive whether the MEP is better than the Pearson system-based method. However, it is observed for our example that including the fifth moment can improve the efficiency in terms of the reduction of total iterations, and the accuracy, which is verified by MCS.

Acknowledgement The research is partially supported by the fund of Samsung Chair Professorship.

References

Ahn JK, Kwon JH (2005) Reliability-based design optimization using trust region-sequential quadratic programming framework. J Aircr 42(5):1331–1336

Athanassoulis GA, Gavriliadis PN (2002) The truncated Hausdorff moment problem solved by using kernel density function. Probab Eng Mech 17:273–291

Chen X, Tung YK (2003) Investigation of polynomial normal transform. Struct Saf 25:423–445

Cover TM, Thomas JA (1991) Elements of information theory. Wiley, New York

D'Errico JR, Zaino NA (1988) Statistical tolerance using modification of Taguchi's method. Technometrics 30(4):397–405

Hahn GJ, Shapiro SS (1968) Statistical models in engineering. Wiley, New York

Hasofer AM, Lind NC (1974) Exact and invariant second order code format. ASCE 100:111–121

Huang D, Du X (2006) Uncertainty analysis by dimension reduction integration and saddlepoint approximations. Trans ASME 128:26–33

Huh JS (2006) Development of a function approximation moment method for reliability analysis and its application to robust optimal design. Ph.D. thesis: Korea Advanced Institute of Science and Technology

Huh JS, Kwak BM (2006) Performance evaluation of precision nano-positioning devices caused by uncertainties due to tolerances using function approximation moment method. Rev Sci Instrum 77:200–209

IMSL (2000) Math Library User's Manual Compaq Visual Fortran 6
Jaynes ET (1957) Information theory and statistical mechanics. Phys Rev 106(4):620–630
Johnson NL, Kotz S, Balakrishnan N (1994) Continuous univariate distributions, vol.1, 2nd edn. Wiley, New York
Ju BH, Lee BC (2007) Improved moment-based quadrature rule and its application to reliability-based design optimization. J Mech Sci Technol 21:1162–1171
Lee SH, Kwak BM (2006) Response surface augmented moment method for efficient reliability analysis. Struct Saf 28: 261–272
Lee SH, Choi HS, Kwak BM (2008) Multi-level design of experiments for statistical moment and probability calculation. Struct Multidisc Optim. doi:10.1007/s00158-007-0215-2
Mead LR, Papanicolaou N (1984) Maximum entropy in the problem of moments. J Math Phys 25(8):2404–2417
Papoulis A, Pillai SU (2002) Probability, random variables, and stochastic processes, 4th edn. McGraw-Hill
Rackwitz R, Fiessler B (1978) Structural reliability under combined random load sequence. Comput Struct 9:489–494
Rahman S, Xu H (2004) A univariate dimension-reduction method for multi-dimensional integration in stochastic mechanics. Probab Eng Mech 19:393–408
Seo HS, Kwak BM (2002) Efficient statistical tolerance analysis for general distributions using three point information. Int J Prod Res 40(4):931–944
Shannon CE (1948) A mathematical theory of communication. Bell Syst Tech J 27:379–423
Stuart A, Ord JK (1994) Kendall's advanced theory of statistics, vol. 1: distribution theory, 6th edn. Oxford, New York
Taguchi G (1978) Performance analysis design. Int J Prod Res 16:521–530
Tu J, Choi KK, Park YH (2001) Design potential method for robust system parameter design. AIAA J 39(4):667–677
Xu H, Rahman S (2005) Decomposition methods for structural reliability analysis. Probab Eng Mech 20:239–250
Zhao YG, Ono T (2000) New point estimates for probability moments. J Eng Mech 126(4):433–436
Zhao YG, Ono T (2001) Moment method for structural reliability. Struct Saf 23:47–75